Science
AAAS

Neoarchean carbonate–associated sulfate records positive $\Delta^{33}S$ anomalies

G. Paris *et al.*

Science **346**, 739 (2014);
DOI: 10.1126/science.1258211

Science (print ISSN 0036-8075; online ISSN 1095-9203) is published weekly, except the last week in December, by the American Association for the Advancement of Science, 1200 New York Avenue NW, Washington, DC 20005.

higher than those of phosphorus. At low concentrations, nutrients such as phosphorus tend to limit biological production, and by analogy, sulfur may have played a more important role as a biologically scarce nutrient.

REFERENCES AND NOTES

1. S. T. Petsch, R. A. Berner, *Am. J. Sci.* **298**, 246–262 (1998).
2. B. B. Jørgensen, *Nature* **296**, 643–645 (1982).
3. D. E. Canfield, *Geochim. Cosmochim. Acta* **65**, 1117–1124 (2001).
4. R. A. Berner, S. T. Petsch, *Science* **282**, 1426–1427 (1998).
5. K. S. Habicht, M. Gade, B. Thamdrup, P. Berg, D. E. Canfield, *Science* **298**, 2372–2374 (2002).
6. Q. J. Guo *et al.*, *Geology* **37**, 399–402 (2009).
7. I. Halevy, D. T. Johnston, D. P. Schrag, *Science* **329**, 204–207 (2010).
8. J. W. Jamieson, B. A. Wing, J. Farquhar, M. D. Hannington, *Nat. Geosci.* **6**, 61 (2013).
9. I. Halevy, *Proc. Natl. Acad. Sci. U.S.A.* **110**, 17644–17649 (2013).
10. J. Farquhar *et al.*, *Proc. Natl. Acad. Sci. U.S.A.* **110**, 17638–17643 (2013).
11. W. W. Fischer *et al.*, *Proc. Natl. Acad. Sci. U.S.A.* **111**, 5468–5473 (2014).
12. B. S. Kamber, M. J. Whitehouse, *Geobiology* **5**, 5–17 (2007).
13. D. E. Canfield, J. Farquhar, A. L. Zerkle, *Geology* **38**, 415–418 (2010).
14. M. L. Gomes, M. T. Hurtgen, *Geology* **41**, 663–666 (2013).
15. M. Nakagawa *et al.*, *Limnol. Oceanogr.* **57**, 974–988 (2012).
16. M. S. Sim, S. Ono, K. Donovan, S. P. Templer, T. Bosak, *Geochim. Cosmochim. Acta* **75**, 4244–4259 (2011).
17. W. D. Leavitt, I. Halevy, A. S. Bradley, D. T. Johnston, *Proc. Natl. Acad. Sci. U.S.A.* **110**, 11244–11249 (2013).
18. S. A. Crowe *et al.*, *Proc. Natl. Acad. Sci. U.S.A.* **105**, 15938–15943 (2008).
19. Materials and methods are available as supplementary materials on *Science* Online.
20. G. Paris, A. L. Sessions, A. V. Subhas, J. F. Adkins, *Chem. Geol.* **345**, 50–61 (2013).
21. M. B. Goldhaber, I. R. Kaplan, *Mar. Chem.* **9**, 95–143 (1980).
22. B. B. Jorgensen, *Geochim. Cosmochim. Acta* **43**, 363–374 (1979).
23. S. Ono *et al.*, *Earth Planet. Sci. Lett.* **213**, 15–30 (2003).
24. S. W. Poulton, D. E. Canfield, *Elements* **7**, 107–112 (2011).
25. D. E. Canfield *et al.*, *Science* **330**, 1375–1378 (2010).
26. E. M. Cameron, K. Hattori, *Chem. Geol.* **65**, 341 (1987).
27. D. E. Canfield, J. Farquhar, *Proc. Natl. Acad. Sci. U.S.A.* **106**, 8123–8127 (2009).
28. I. B. Lambert, T. H. Donnelly, J. S. R. Dunlop, D. I. Groves, *Nature* **276**, 808–811 (1978).
29. D. L. Roerdink, P. R. D. Mason, J. Farquhar, T. Reimer, *Earth Planet. Sci. Lett.* **331–332**, 177–186 (2012).
30. E. E. Stüeken, D. C. Catling, R. Buick, *Nat. Geosci.* **5**, 722–725 (2012).
31. C. T. A. Chen, C. M. Lin, B. T. Huang, L. F. Chang, *Mar. Chem.* **54**, 179–190 (1996).
32. S. A. Crowe *et al.*, *Geobiology* **12**, 322–339 (2014).

ACKNOWLEDGMENTS

We thank A. Sturm and C. Henny for help with fieldwork. S. Poulton provided sediment $\delta^{34}S$ data. A. Hefford helped compile Archean S-isotope data. Funding to S.A.C. was provided by an Agouron Institute Geobiology Fellowship and a *Natural Sciences and Engineering Research Council* of Canada Postdoctoral Fellowship. Additional funding was provided by the Danish National Research Foundation (grant no. DNRF53) and the European Research Council. All data are available in the supplementary materials.

SUPPLEMENTARY MATERIALS

www.sciencemag.org/content/346/6210/735/suppl/DC1
Materials and Methods
Supplementary Text
Figs. S1 and S2
Tables S1 to S5
References (*33*–*68*)
Data S1

21 July 2014; accepted 10 October 2014
10.1126/science.1258966

EARLY EARTH

Neoarchean carbonate-associated sulfate records positive $\Delta^{33}S$ anomalies

G. Paris,[1]* J. F. Adkins,[1] A. L. Sessions,[1] S. M. Webb,[2] W. W. Fischer[1]

Mass-independent fractionation of sulfur isotopes (reported as $\Delta^{33}S$) recorded in Archean sedimentary rocks helps to constrain the composition of Earth's early atmosphere and the timing of the rise of oxygen ~2.4 billion years ago. Although current hypotheses predict uniformly negative $\Delta^{33}S$ for Archean seawater sulfate, this remains untested through the vast majority of Archean time. We applied x-ray absorption spectroscopy to investigate the low sulfate content of particularly well-preserved Neoarchean carbonates and mass spectrometry to measure their $\Delta^{33}S$ signatures. We report unexpected, large, widespread positive $\Delta^{33}S$ values from stratigraphic sections capturing over 70 million years and diverse depositional environments. Combined with the pyrite record, these results show that sulfate does not carry the expected negative $\Delta^{33}S$ from sulfur mass-independent fractionation in the Neoarchean atmosphere.

The sulfur isotopic composition of Archean [3.8 to 2.4 billion years ago (Ga)] sedimentary rocks provides critical evidence that Earth's atmosphere contained very little, if any, free O_2 before the rise of oxygen ~2.4 Ga (*1*–*6*). Most processes on Earth fractionate sulfur isotopes proportionally to their relative mass differences [$\Delta^{33}S = 0$ (*7*)], yet Archean pyrite (FeS_2) commonly deviates from this relationship, skewed toward positive $\Delta^{33}S$ values (*1*, *8*). This mass-independent fractionation (MIF) pattern is widely attributed to photodissociation of SO_2 by ultraviolet (UV) light allowed by the extremely low levels of O_2 and O_3 in Earth's atmosphere at that time (*1*, *6*). In this scenario, coeval sulfate aerosols ultimately deposited in the ocean as dissolved sulfate carry the complementary negative $\Delta^{33}S$ anomalies required by isotopic mass balance (*1*, *2*, *5*, *8*, *9*). Recent experiments (*10*–*12*) and models of the Archean atmosphere (*2*) show a much wider range of MIF patterns, including positive $\Delta^{33}S$ anomalies in sulfate instead of lower-valent S species. Sulfate minerals that would provide a test of the distribution of MIF signal are absent from Archean evaporite sequences—bedded sulfate deposits occur only after the rise of oxygen (*13*). Paleoarchean barites (3.5 to 3.2 Ga) are a notable exception. They carry small, negative $\Delta^{33}S$ values [0 to −1.5‰ (*1*, *14*–*16*)] but have an enigmatic petrogenesis (*17*). No such sulfate record exists for the billion-year interval from Mesoarchean time through the Paleoproterozoic rise of oxygen. Consequently, the notion of an Archean marine sulfate pool with negative $\Delta^{33}S$ values remains largely untested.

Sulfate minerals are not the only portal into the past marine sulfate pool. Small quantities of carbonate-associated sulfate (CAS) have become an important archive for studying marine sulfate in younger successions (*18*). However, the very low sulfate concentrations of Archean carbonates have kept this archive largely out of reach for conventional analytical methods. Two studies measuring Archean CAS suggested that Archean sulfate carried positive $\Delta^{33}S$ (*4*, *19*). However, both studies used large sample sizes (>100 g of $CaCO_3$), raising the risks of lower preservation as well as contamination by pyrite. We recently developed a technique using inductively coupled plasma mass spectrometry to measure both $\Delta^{33}S$ and $\delta^{34}S$ using a few tens of milligrams of low-CAS carbonate (*20*). Greater sensitivity allows the measurement of sulfur isotopes from specific petrographic and sedimentary fabrics with different diagenetic histories, coupled with light and electron microscopy (Fig. 1 and fig. S4), to directly assess sample quality based on the presence of additional S-bearing phases (e.g., organic sulfur, pyrite). In parallel, we applied synchrotron x-ray absorption spectroscopy (XAS) to measure sulfur speciation in these samples. We examined three sedimentary sections from a range of marine paleoenvironments across the Neoarchean Campbellrand carbonate platform (*21*). Section W1 (aragonite sea-floor fans, precipitated laminae, preserved as early diagenetic fabric-retentive dolomite) captures shallow subtidal environments, whereas sections GKP01 and W2 [herringbone, an early marine calcitic cement (*22*), microbial laminae, dolomite, and calcite spar] capture deep subtidal and slope environments (*21*).

The CAS data preserve positive $\delta^{34}S$ values and unambiguously positive $\Delta^{33}S$ values and display significant variability, sometimes at very small scales (Fig. 2 and additional data table S1). The carbonate fabrics contain 5 to 70 parts per million (ppm) sulfate—two orders of magnitude lower than typical Phanerozoic carbonates. Because of such low levels, we consider the potential impacts of contamination and/or sulfide oxidation

[1]Division of Geological and Planetary Sciences, California Institute of Technology, Pasadena, CA 91125, USA. [2]Stanford Synchrotron Radiation Lightsource, Menlo Park, CA 94025, USA.
*Corresponding author. E-mail: gparis@caltech.edu

on these measurements. Contamination by post-Archean sulfur of any form, in the laboratory or field, can be confidently ruled out because it would not carry a substantial MIF signal. Modern oxidation of indigenous pyrite or organic sulfur would carry such a signal, although our sample-cleaning protocol is designed to extract only the sulfate bound into the carbonate lattice (*21*). Late, void-filling calcite spar is notable for having extremely low sulfate concentrations (≤4.3 ppm) and so provides an important negative control. XAS analyses of samples prepared under strictly anaerobic conditions indicate an average of 22 (±14%) sulfate S, 67 (±13%) pyrite S, and 12 (±7%) organic S [(*21*); table S3 and fig. S5] and show that there is an appreciable amount of sulfate present. At worst, our analyses represent a mixture of CAS and oxidized pyrite, yet plots of either $\delta^{34}S$ or $\Delta^{33}S$ versus concentration show no correlation (fig. S8), as would be expected for such a mixture. Moreover, the mean $\Delta^{33}S$ value for CAS is higher than that for coeval disseminated pyrite (*4*, *23*–*30*), averaging 6.39 and 4.48‰, respectively (fig. S9). Although we cannot rule out a heterogeneous distribution of pyrite grains, with smaller, easier-to-oxidize grains carrying larger-than-average $\Delta^{33}S$ values, this should still lead to a correlation between sulfate concentration and $\Delta^{33}S$.

A possibility that is more difficult to rule out is the existence of an ancient fluid-flow event that oxidized pyrite while simultaneously recrystallizing carbonate minerals. The absence of measurable sulfate in void-filling sparry cements argues against this possibility, as do variable sulfate concentrations between closely colocated carbonate fabrics. Carbon and oxygen isotopic compositions are consistent with previously reported values and are inconsistent with extensive interaction with hydrothermal fluids (*31*). There is no correlation between $\delta^{34}S$ or $\Delta^{33}S$ and either carbon or oxygen isotope ratios (fig. S10), as might be expected of a diagenetic origin for sulfate. Lastly, the carbonates contain substantially more reduced iron (0.5 to 1%) than reduced sulfur (<0.1%), yet no detectable oxidized iron (*32*). Such a pattern is inconsistent with any diagenetic event that locally oxidized pyrite. We conclude that the measured CAS represents Neoarchean marine sulfate with a strong positive $\Delta^{33}S$ anomaly.

Our data challenge the canonical view of the Archean sulfur cycle in which S_8 compounds with positive $\Delta^{33}S$ values and SO_4^{2-} with negative $\Delta^{33}S$ values derived from SO_2 photolysis to form the reduced and oxidized pools of sulfur, respectively. In Fig. 3A, we compare the sulfur isotopic compositions as normalized ratios $\delta'^{33}S$ and $\delta'^{34}S$ (*7*) of CAS against an extensive set of published values from Campbellrand platform pyrites. If sulfate originated from pyrite oxidation, CAS should overlap pyrites and show both negative and positive $\Delta^{33}S$ values. Instead, we observe that the $\delta'^{34}S$ values of CAS and disseminated pyrite complement each other, which provides a simple framework to interpret previously published data. Microbial sulfate reduction produces pyrite

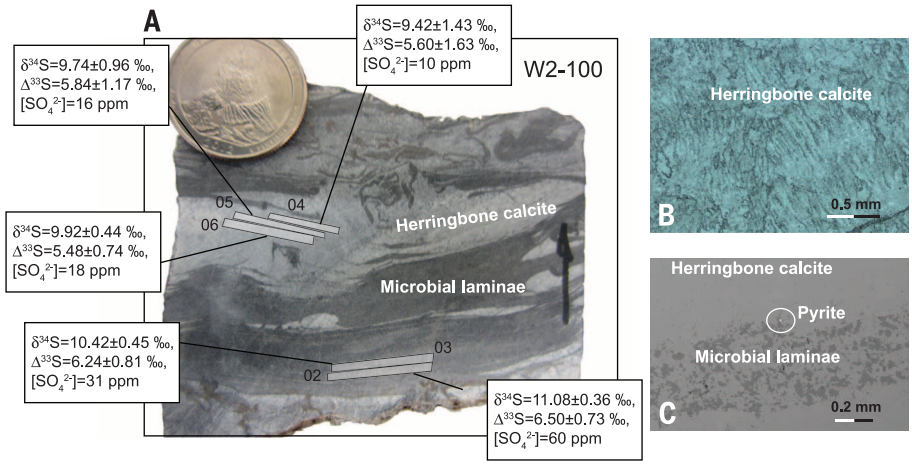

Fig. 1. Measurement of multiple sulfur isotope ratios from specific petrographic textures within a sample. (**A**) Cut face of hand sample W2-100 contains several different calcite fabrics, dark microbial laminae, and marine herringbone calcite cements. Sample locations are shown as numbered light gray areas. U.S. quarter is shown for scale. (**B**) Transmitted light and (**C**) backscatter electron photomicrographs of a thin section facing the location of samples 4 to 6. Herringbone calcite generally lacks reflective (or high backscatter) sulfide-bearing minerals, whereas microbial laminae textures may contain rare small (~2 μm) pyrite grains.

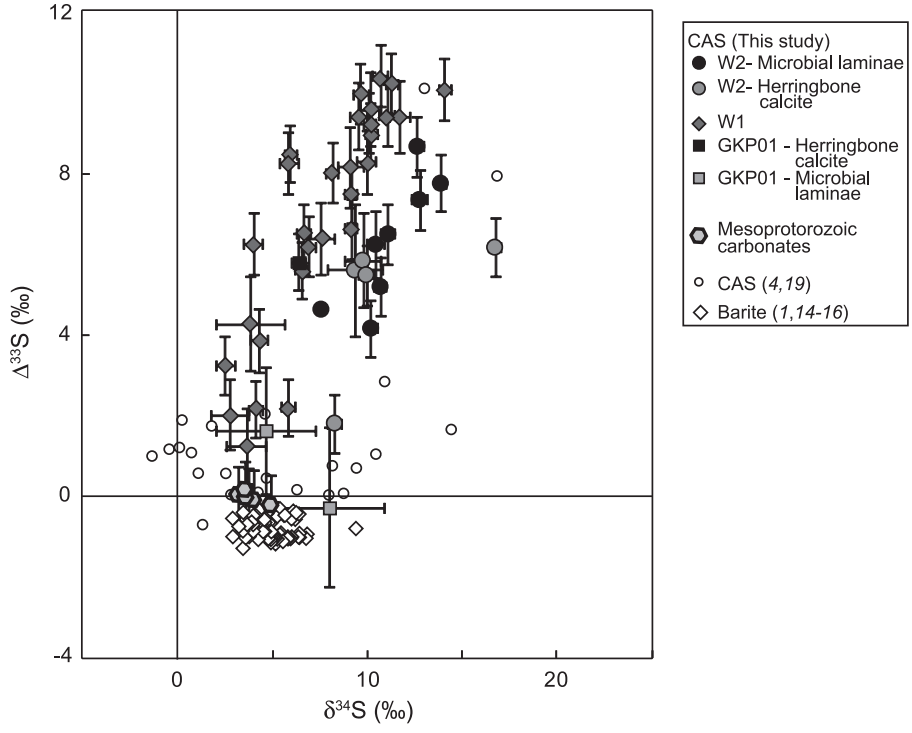

Fig. 2. Crossplot of $\delta^{34}S$ versus $\Delta^{33}S$ values for all Archean sulfate measured to date. CAS [Campbellrand carbonate platform, 2.6 to 2.5 Ga, this study, mean ± 2 SD (*4*, *21*), and various locations, 3.0 to 2.6 Ga (*19*)] and the Paleoarchean barite record (*1*, *14*–*16*). For comparison, CAS data from the Mesoproterozoic-age Helena Formation measured in this study are shown; note the lack of MIF in these samples (after the rise of oxygen).

with the same $\Delta^{33}S$ as, and lower $\delta^{34}S$ than, sulfate. In Fig. 3A, this MIF is expressed as vectors parallel to the dashed line toward the left, which explains most of the disseminated pyrite. To explain the few ^{34}S-enriched pyrites, either porewater sulfate must have become enriched in ^{34}S over the course of sulfate reduction [as in modern anoxic pore waters (*33*)], or additional mass-dependent processes were involved. The overall fractionation leaves the remaining dissolved sulfate pool slightly enriched in heavy isotopes within the Campbellrand basin, moving the $\delta^{34}S$-intercept of the fractionation line above the origin of the $\delta^{34}S$-$\Delta^{33}S$ crossplot (Fig. 2).

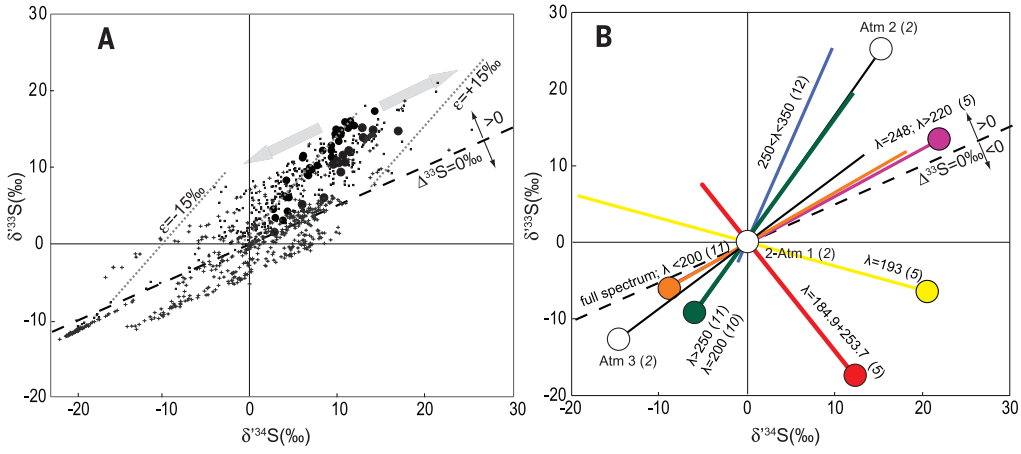

Fig. 3. Comparison between sulfur isotopic compositions in data and laboratory and numerical experiments. (**A**) Comparison of sulfur isotope composition for CAS (this study, circles) and pyrite [disseminated, dots; nodule and layers, crosses (*4*, *23*–*30*, *33*)] from the Campbellrand platform. The CAS data define a narrow range, departing from bulk Earth sulfur (the origin on this plot) by MIF processes. Dashed line is the mass-dependent (MD) fractionation law. Disseminated pyrite isotopic compositions depart from the CAS trend via MD processes (gray arrows). Dotted lines indicate the MIF law for section W1 with no fractionation and with MD fractionations (ε) of –15 and +15‰. The Neoarchean pyrite record from South Africa also includes pyrites, mostly nodular, with negative $\Delta^{33}S$ values. (**B**) Mass fractionation laws for published photochemistry experiments at different wavelengths λ (nm) or atmospheric compositions. The slope of each line is the average mass law centered on the origin for a given data set. The circles indicate the oxidized sulfur endmember, close to which are reported the wavelengths used for each experiment. Atm 1, 2, and 3 are Archean theoretical atmospheres 1, 2, and 3 (*2*).

Nodular pyrites (*25*–*27*, *29*, *33*) commonly display a negative $\Delta^{33}S$ signature, shown below the dashed line in Fig. 3A. Rather than marine sulfate, these pyrites could be representative of a sulfur pool mass-balancing the Archean sulfur cycle (*1*, *2*, *8*, *14*, *29*).

The small-scale variation observed in $\Delta^{33}S$ values within samples may reflect the atmospheric processes that create MIF. In the modern world, the $\Delta^{33}S$ of sulfate aerosols produced after volcanic injections of SO_2 into the stratosphere changes within a few years (*34*). Therefore, atmospheric fractionations, but also output fluxes, can vary on time scales much shorter than the temporal resolution of the stratigraphic record. Because atmospheric processes create MIF that follow a linear trend in the $\delta'^{33}S$-$\delta'^{34}S$ space, the observation of a slope between $\Delta^{33}S$ and $\delta^{34}S$ values supports this notion. The small-scale variation could also reflect differing extents of sulfur cycling between different coeval pools (elemental sulfur, sulfide, etc.) (*33*, *35*). Regardless, these possibilities each point to relatively low concentrations, a short residence time of seawater sulfate in this marine basin, and limited exchange between sulfur pools to prevent $\Delta^{33}S$ homogenization (*35*).

Existing models of Archean sulfur cycling were influenced by early experimental results for SO_2 interaction with UV light that produced oxidized species with negative $\Delta^{33}S$ values (*5*). In Fig. 3B, we compile all the results from experimental work (*5*, *8*–*12*) and atmospheric modeling (*2*) exploring sulfur isotope MIF trends. We derive mass fractionation laws, defined as the slope between the normalized ratios $\delta'^{33}S$ and $\delta'^{34}S$ (*7*) for the products of atmospheric processes either in the laboratory or in simulations of the Archean atmosphere. The oxidized sulfur products are marked at the ends of the mass fractionation lines with circles. The mass laws for these different experiments display a broad range of slopes, and different signs of $\Delta^{33}S$ for SO_4^{2-}. Recent studies (*2*, *10*–*12*) show more scenarios in which the oxidized sulfur pool resulting from SO_2 photochemistry bears positive $\Delta^{33}S$ values (Fig. 3B). More broadly, time series of records of sulfur isotopes in Archean carbonates can now provide a key test for hypotheses derived from experiments and theory regarding the composition and evolution of Earth's early atmosphere.

REFERENCES AND NOTES

1. J. Farquhar, H. Bao, M. Thiemens, *Science* **289**, 756–758 (2000).
2. Y. Ueno *et al.*, *Proc. Natl. Acad. Sci. U.S.A.* **106**, 14784–14789 (2009).
3. A. Bekker *et al.*, *Science* **326**, 1086–1089 (2009).
4. Q. Guo *et al.*, *Geology* **37**, 399–402 (2009).
5. J. Farquhar, J. Savarino, S. Airieau, M. H. Thiemens, *J. Geophys. Res. Planets* **106**, 32829 (2001).
6. A. A. Pavlov, J. F. Kasting, *Astrobiology* **2**, 27–41 (2002).
7. Isotopic ratios are usually reported as $\delta^{3x}S$ (3*x* being either 33, 34, or 36) values where $\delta^{3x}S = 1000 \times [(^{3x}S/^{32}S)_{sample}/(^{3x}S/^{32}S_{VCDT}) - 1] \times 1000$. The terrestrial mass fractionation law is conventionally defined as $\delta'^{33}S = 0.515 \times \delta'^{34}S$, where $\delta'^{3x}S = 1000 \times \ln[(^{3x}S/^{32}S)_{sample}/(^{3x}S/^{32}S_{VCDT})]$ with VCDT the Vienna Canyon Diablo Troilite reference standard. Deviations from this relationship are commonly termed "mass-independent fractionation" and are quantified as $\Delta^{33}S = \delta'^{33}S - 0.515 \times \delta'^{34}S$.
8. I. Halevy, D. T. Johnston, D. P. Schrag, *Science* **329**, 204–207 (2010).
9. J. R. Lyons, *Geophys. Res. Lett.* **34**, L22811 (2007).
10. A. L. Masterson, J. Farquhar, B. A. Wing, *Earth Planet. Sci. Lett.* **306**, 253–260 (2011).
11. A. R. Whitehill, S. Ono, *Geochim. Cosmochim. Acta* **94**, 238–253 (2012).
12. A. R. Whitehill *et al.*, *Proc. Natl. Acad. Sci. U.S.A.* **110**, 17697–17702 (2013).
13. J. P. Grotzinger, J. F. Kasting, *J. Geol.* **101**, 235–243 (1993).
14. H. Bao, D. Rumble III, D. R. Lowe, *Geochim. Cosmochim. Acta* **71**, 4868–4879 (2007).
15. Y. Ueno, S. Ono, D. Rumble, S. Maruyama, *Geochim. Cosmochim. Acta* **72**, 5675–5691 (2008).
16. D. L. Roerdink, P. R. D. Mason, J. Farquhar, T. Reimer, *Earth Planet. Sci. Lett.* **331–332**, 177–186 (2012).
17. M. J. Van Kranendonk, *Earth Sci. Rev.* **74**, 197–240 (2006).
18. L. C. Kah, T. W. Lyons, J. T. Chesley, *Precambrian Res.* **111**, 203–234 (2001).
19. S. D. Domagal-Goldman, J. F. Kasting, D. T. Johnston, J. Farquhar, *Earth Planet. Sci. Lett.* **269**, 29–40 (2008).
20. G. Paris, A. L. Sessions, A. V. Subhas, J. F. Adkins, *Chem. Geol.* **345**, 50–61 (2013).
21. Materials and methods are available on *Science* Online.
22. D. Y. Sumner, J. P. Grotzinger, *J. Sediment. Res.* **66**, 419 (1996).
23. G. Hu, D. Rumble, P.-L. Wang, *Geochim. Cosmochim. Acta* **67**, 3101–3118 (2003).
24. A. J. Kaufman *et al.*, *Science* **317**, 1900–1903 (2007).
25. S. Ono, N. J. Beukes, D. Rumble, *Precambrian Res.* **169**, 48–57 (2009).
26. B. S. Kamber, M. J. Whitehouse, *Geobiology* **5**, 5–17 (2007).
27. S. Ono, A. J. Kaufman, J. Farquhar, D. Y. Sumner, N. J. Beukes, *Precambrian Res.* **169**, 58–67 (2009).
28. D. Papineau, S. J. Mojzsis, *Geobiology* **4**, 227–238 (2006).
29. J. Farquhar *et al.*, *Proc. Natl. Acad. Sci. U.S.A.* **110**, 17638–17643 (2013).
30. A. L. Zerkle, M. W. Claire, S. D. Domagal-Goldman, J. Farquhar, S. W. Poulton, *Nat. Geosci.* **5**, 359–363 (2012).
31. W. W. Fischer *et al.*, *Precambrian Res.* **169**, 15–27 (2009).
32. N. J. Beukes, *Sediment. Geol.* **54**, 1–46 (1987).
33. W. W. Fischer *et al.*, *Proc. Natl. Acad. Sci. U.S.A.* **111**, 5468–5473 (2014).
34. M. Baroni, M. H. Thiemens, R. J. Delmas, J. Savarino, *Science* **315**, 84–87 (2007).
35. I. Halevy, *Proc. Natl. Acad. Sci. U.S.A.* **110**, 11244–11249 (2013).

ACKNOWLEDGMENTS

We thank J. Johnson for help with stratigraphic sample collection and fruitful comments; N. Beukes and I. Halevy for helpful discussions; K. Bergmann for assistance with C and O analyses; and C. Ma, T. Present, and J. Johnson for assistance with scanning electron microscopy. We acknowledge support from NSF Division of Earth Sciences award no. EAR-1349858. Assistance from N. Dalleska and use of IC instrumentation in the Environmental Analysis Center at the California Institute of Technology is gratefully acknowledged. G.P. was funded by the Henry and Camille Dreyfus Postdoctoral Program in Environmental Chemistry. W.W.F. acknowledges support from the David and Lucile Packard Foundation. Drill core GKP01 was sampled with support from the Agouron Institute. Use of the Stanford Synchrotron Radiation Lightsource, SLAC National Accelerator Laboratory, is supported by the U.S. Department of Energy, Office of Science, Office of Basic Energy Sciences under Contract No. DE-AC02-76SF00515. The SSRL Structural Molecular Biology Program is supported by the DOE Office of Biological and Environmental Research and by the National Institutes of Health, National Institute of General Medical Sciences (including P41GM103393).

SUPPLEMENTARY MATERIALS

www.sciencemag.org/content/346/6210/739/suppl/DC1
Materials and Methods
Figs. S1 to S10
Tables S1 to S3
References (*36*–*54*)
Additional Data Table S1

2 July 2014; accepted 22 September 2014
10.1126/science.1258211